REPORT DOCUMENTATION PAGE

Public Reporting burden for this collection of information is estimated to average 1 hour per response, including the time for reviewing instructions, searching existing data sources, gathering and maintaining the data needed, and completing and reviewing the collection of information. Send comment regarding this burden estimates or any other aspect of this collection of information, including suggestions for reducing this burden, to Washington Headquarters Services, Directorate for information Operations and Reports, 1215 Jefferson Davis Highway, Suite 1204, Arlington, VA 22202-4302, and to the Office of Management and Budget, Paperwork Reduction Project (0704-0188,) Washington, DC 20503.

1. AGENCY USE ONLY (Leave Blank)	2. REPORT DATE February 26, 2004	3. REPORT TYPE AND DATES COVERED **Final 3/19/01 to 09/30/2003**

4. TITLE AND SUBTITLE **Experiments on Polymer Drag Reduction Using PIV and PLIF**	5. FUNDING NUMBERS **MDA972-01-C-0022**
6. AUTHOR(S) **M. G. Mungal**	

7. PERFORMING ORGANIZATION NAME(S) AND ADDRESS(ES) **Stanford University Mechanical Engineering Department Thermoscience Division, Stanford, CA 94305-3030**	8. PERFORMING ORGANIZATION REPORT NUMBER

9. SPONSORING / MONITORING AGENCY NAME(S) AND ADDRESS(ES) **Defense Advanced Research Projects Agency (DARPA) Contracts Management Office (CMO) Attn: Mr. Charles N. Nurse 3701 North Fairfax Drive Arlington, VA 22203-1714**	10. SPONSORING / MONITORING AGENCY REPORT NUMBER **Office of Naval Research Office Ballston Centre Tower One Arlington, VA 22217-5660**

11. SUPPLEMENTARY NOTES

The views, opinions and/or findings contained in this report are those of the author(s) and should not be construed as an official Department of the Army position, policy or decision, unless so designated by other documentation.

12 a. DISTRIBUTION / AVAILABILITY STATEMENT Approved for public release; distribution unlimited.	12 b. DISTRIBUTION CODE

13. ABSTRACT (Maximum 200 words)

The structure of turbulence in a drag reduced flat plate boundary layer has been studied with particle image velocimetry (PIV) and planar laser induced fluorescence (PLIF). Drag reduction was achieved by injection of a solution of water-soluble polymer through a spanwise slot near the leading edge of the flat plate. Velocity and concentration data were obtained using PIV and PLIF, respectively, in planes parallel to the wall (x-z plane) and perpendicular to the wall (x-y plane). Measurements of velocity, vorticity and streak spacing were obtained and trends analyzed. For increasing drag reduction, damping of streak oscillations, suppression of streak splitting and merging, streak stabilization and coarsening of the low speed streaks was observed. PLIF measurements of the injected polymer solution showed that regions of high polymer concentration are correlated with the low speed streaks. PIV measurements in the x-y plane showed that at Maximum Drag Reduction (MDR) there are significant differences in the statistics of turbulence between boundary layers with polymer injection and channel flow with an ocean of polymer suggesting that in this sense, the achievement of MDR in flows with polymer addition is not unique.

14. SUBJECT TERMS Drag Reduction; Polymer addition; Turbulent boundary layer; PIV; PLIF			15. NUMBER OF PAGES 14
			16. PRICE CODE

17. SECURITY CLASSIFICATION OR REPORT UNCLASSIFIED	18. SECURITY CLASSIFICATION ON THIS PAGE UNCLASSIFIED	19. SECURITY CLASSIFICATION OF ABSTRACT UNCLASSIFIED	20. LIMITATION OF ABSTRACT UL

NSN 7540-01-280-5500

Best Available Copy

20040305 011

Final Technical Report

Experiments on Polymer Drag Reduction Using PIV and PLIF

M. G. Mungal
Mechanical Engineering Department
Stanford University, Stanford, CA 94305

Task Objects

Drag reduction by polymer injection is a phenomenon which has been known for over 50 years. However the detailed mechanisms leading to such are not presently well understood. To this end drag reduction on a flat plate boundary layer by use of polymer injection was layer was investigated. Here, polymer was injected into the sublayer region of the flow and detailed Particle Image Velocimetry (PIV) and Planar Laser Induced Fluorescence (PLIF) measurements were performed. PIV was able to document the important changes to the flow with polymer addition, while PLIF was able to show the concentration of polymer within the boundary layer at the measurement location. Experiments were performed at a single axial station located well downstream of the injection station. The results are used for comparison with an ongoing set of computations of the same phenomenon.

Technical Problems

PIV is a challenging technique for application to wall bounded flows. The main problem concerns the adequacy of the spatial resolution achievable by the technique, and the wall reflections from the laser sheet used which can compromise the measurement accuracy. In addition, PLIF requires the use of a fluorescent which should largely track the injected polymer. Both of these problems were solved adequately as is described in the Technical Results section.

General Methodology

The dilute addition of long chain polymers to wall bounded flows can produce substantial reductions in skin friction when compared to their Newtonian counterparts. As a consequence of a reduction in the wall friction, the mean velocity profile will be modified, which in turn modifies the structure of turbulence near the wall. Therefore, an important part of understanding the mechanism of polymer drag reduction is to measure the effect of polymer on the near wall structure of turbulence.

While past studies [1, 2] have elucidated, to some degree, the action of the polymer in the boundary layer, there is a lack of quantitative turbulence data on the effect of polymer on the structure of turbulence. Moreover there are even fewer measurements taken in a boundary layer flow [3]. The present study is an attempt to correct both deficiencies. In the present study, the structure of turbulence in a zero pressure gradient boundary layer flow very close to the wall ($y^+ \sim 10$) is measured using PIV. The data presented here provides a quantitative measure of the polymer effects on the structure of turbulence in the near wall region. The data can also be used to validate models used for simulating polymer drag reduction and help in formulating new models that better capture the physics of polymer drag reduction. A similar effort, but in a channel flow with homogeneous polymer concentration was done by Warholic et al [4].

Boundary layer flow facility

The experiments are conducted in a constant head closed circuit water tunnel as shown in Figure 1. The boundary layer test surface is the upper wall of the tunnel. Manual valves along the lower and side walls of the tunnel are adjusted accordingly to maintain a zero pressure gradient condition along the upper test wall. The test section has a cross section of 36 cm in span and 13 cm in height with a length of 3.66 m. The walls

are constructed of plexiglass to provide full optical access to the flow. The inlet velocity ranges from 0.3 to 0.7 ms^{-1}. The water in the tunnel is maintained at a constant temperature using a refrigerated chiller, and a cyclone type de-aeration system is used to remove air from the water. The leading edge of the test wall is a half elliptical nose with an axes ratio of 16. A wire of 0.13mm diameter, located 13 cm downstream of the leading edge, is used to trip the boundary layer and make it turbulent. Polymer injection into the boundary layer is carried out using a span-wise slot of width 0.15mm, located 2 cm downstream of the trip wire. A more detailed description of the water tunnel is given in [5].

At the start of an experiment, the tunnel is filled with water carefully to avoid entrapment of air on the test wall, and any remaining air is removed using the de-aeration system by running the tunnel for several hours before measurements are taken. Once the air is removed and water temperature is constant, the required velocity is set and a zero pressure gradient condition is achieved by adjusting the manual bleed valves on the lower and side walls. A zero pressure gradient condition is verified by obtaining multiple velocity measurements at several locations in the streamwise direction and ensuring that $dU/dx = 0$. PIV and PLIF data in the boundary layer is obtained at a location 2m downstream of the leading edge as the boundary layer is the thickest there and the resolution is the best.

Wall friction measurements are made with thermal and optical shear stress sensors 6 cm downstream of the PIV measurement station. The thermal shear stress probes used are TSI 1268W hot film probes flush mounted on the test wall and calibrated in the boundary layer. The optical sensor is a Viosense S^3 micro shear stress sensor. This sensor works by measuring the velocity gradient at the wall as described in [6].

The polymer used is poly(ethylene oxide) (PEO) with a mean molecular weight of 3.8 million and a poly-dispersity of 1.5. The polymer solution is prepared by mixing a carefully weighed amount of PEO with ethylene glycol and then dripped slowly down the side of a container with water used to wash it into solution. The ethylene glycol is used to prevent agglomeration of the polymer particles as they are mixed with water. After the polymer is added to the water, the solution is gently stirred for several hours to ensure homogeneity and then left to stand for 24 hours before it is used in the experiment.

The polymer solution (or water) is injected into the boundary layer by pressurizing its container slightly above the pressure in the channel (~6psig). A small plenum chamber located above the slot injector is used to equilibrate pressure and provide uniform flow across the span of the slot. Different drag reductions are obtained by varying the injection rate of the polymer solution by varying the container overpressure. Injection times vary between 20-30 minutes depending upon the injection rates, and, over this period, the drag remains steady as measured by the shear stress sensors implying that recirculated polymer is destroyed by the tunnel pump.

Particle image velocimetry measurements

The Particle Image Velocimetry (PIV) measurements in the x-z plane are made using a 12 bit CCD camera with a resolution of 1280 x 1012 pixels, a dual head, pulsed Nd:YAG laser operating at 532nm and sheet forming optics. A schematic of the PIV measurement station for the x-z plane is shown in figure 2. The camera and the sheet forming optics are mounted on a translation stage that moves the system normal to the

3

test surface with a resolution of 12.7μm. At a fixed streamwise location, PIV images are obtained for 30 planes across the thickness of the boundary layer. These measurements are made in sets of 10 planes; the first set, closest to the wall, has a separation of 0.127mm between each plane, 0.508mm for the next set and 3.81mm for the final. For the 10 planes closest to the wall, 50 images are acquired per plane and 20 images per plane are acquired for the remainder.

PIV measurements in the x-y plane are made using the same equipment as used for measurement in the xz plane but with a modified setup as shown in figure 3. Six hundred images are taken at a fixed position that spans, in the wall normal direction, from the wall to 1.38 cm. The PIV images are analyzed using the cross-correlation technique with multi-passing [7]. The first pass is over a box of 64x64 pixels with no overlap of adjacent boxes and the second pass is over a 32x32 box with 50% overlap. A second order correlation scheme similar to that described in [8] is used on the second pass to improve the signal to noise ratio in the correlation plane. Validation of the vector field is done using a local median filter [14]. A vector determined to be spurious is either left blank or replaced with one corresponding to a secondary correlation peak in the correlation plane. The tracer particles used to seed the flow are 0.5-2μm glass spheres, and their loading is such that there is an average of 10 particles in a 32x32 pixel area.

In the x-z plane, vector yield close to the wall ($y^+ < 50$) is typically 90-95% and about 99% in the remainder of the flow. Spatial resolution of the camera is 20μm per pixel. This gives an effective field of view of 2.6 cm x 2.0 cm with a small scale resolution of 640μm. In the x-y plane, spatial resolution of the camera is 13.4 μm per pixel with an effective field of view of 17.2 cm x 13.6 cm. The small scale resolution in this plane is 430 μm.

Validation of the PIV system and data analysis in the boundary layer flow is performed at two momentum thickness Reynolds numbers, $R_\theta = U\theta/\nu$, of 1100 and 1400 where U is the freestream velocity, θ is the momentum thickness of the boundary layer and ν is the kinematic viscosity of water. All drag reduction measurements are done at R_θ between 1300 and 1500.

Planar laser induced fluorescence measurements

Simultaneous planar laser induced fluorescence (PLIF) and PIV measurements are carried out, in the x-y plane, using the setup shown in Figure 3. The PLIF camera is mounted opposite to the PIV camera and care is taken to ensure that both cameras image the same position of space in the tunnel to within 2 pixels. Rhodamine WT is used as the dye for the PLIF experiments to visualize the spatial distribution and concentration of the polymer in the boundary layer. A measured amount of dye is mixed into the polymer solution to give a final concentration of 1.6×10^{-6} mol/litre. As rhodamine WT fluoresces at 640 nm, a Schott glass filter, OG-570, is used to allow only the PLIF signal. A sample of the injected solution is used for calibration purposes.

Technical Results

Shear stress measurements

A thermal hot film wall shear stress sensor is used to measure the shear stress in the boundary layer at $R_\theta = 1400$ in water for the case of no injection, water injection and

injection of 500ppmw PEO solution. The voltage signal obtained from the sensor is shown in figure 4. In figure 4(a), the mean shear stress for the case of no injection and with water injection is plotted and shows that the wall friction is virtually unchanged by the injection of water. This indicates that the injection of fluid has no effect on the downstream boundary layer (velocity measurements also show the same effect). Hence, any effect observed with polymer injection is solely due to the action of polymer. Figure 4(b) shows the shear stress sensor voltage output for the case on no injection and the injection of a concentrated polymer solution. For the case of polymer injection, regions I, II and III correspond to parts of the signal obtained prior to, at the start of, and during steady state injection of the fluid into the boundary layer, respectively. The injection rates of both water and polymer are approximately 5 times the volumetric flow rate of the linear sublayer assuming a sublayer thickness of $y^+ = 5$.

PIV in the x-z plane

The experiment is first conducted for the case of no fluid injection into the boundary layer. PIV measurements are made at a fixed streamwise location for 30 planes spanning the thickness of the boundary layer. The plane closest to the wall is at $y \approx$ 0.5mm. In the next experiment, water is injected into the boundary layer at the same flow rate at which polymer solution will be injected. Shear stress at the wall is monitored before, during and after injection. PIV data acquisition is started when the shear stress signal becomes constant after the start of injection. For drag reduction experiments, a polymer solution with concentrations between 100 and 1000 ppmw is injected into the boundary layer and shear stress and PIV data are obtained as described for the case of water injection.

PIV measurements are acquired for four percentages of drag reductions of 33%, 45%, 50% and 67% with the properties of the boundary layer at these drag reductions listed in Table 1. Also given are the injected polymer concentration (C_i) and the homogenous polymer concentration (C_h) which is the concentration if the injected polymer is fully mixed into the entire channel. Figure 5 shows typical PIV vector plots of the fluctuating velocity obtained for 0% and 45% drag reductions. Turbulence statistics for each plane are obtained by ensemble averaging over the total number of images acquired for that plane. Figure 6 shows the mean velocity profile in wall coordinates for water and three drag reductions. The mean velocity profile for water shows the expected behavior in the log law region, $30 < y^+ < 150$, denoted by (ii). The mean velocity profiles for the drag reduced flows are consistent with previous studies. At low drag reduction (33%), a vertical shift in the log region and a thickening of the buffer layer are observed. At higher drag reductions, 45% and 67%, the slope of the log layer is different and the profile itself is different from that of a Newtonian one. The line (iii) denotes the empirical upper bound for polymer drag reduction as classified by Virk [9].

The root mean square velocity profiles for the streamwise (u'^+) and the spanwise (w'^+) components are shown in figure 7 for water and for the different drag reduction cases. The data obtained for water is consistent with DNS data of Spalart [10] at $R_\theta =$ 1410. For polymer drag reduced flow, the peak in the streamwise velocity fluctuation profile increases and moves away from the wall with increasing drag reduction. This is consistent with Warholic et al [11], except at the highest drag reduction case of 67% (near MDR). Their experiments have noted a decrease in the magnitude of the peak to

values less than or equal to that observed in water. The spanwise fluctuations are lower than those observed in water for all drag reductions in the present work and these are in agreement with previous studies.

Two dominant structures of near wall turbulence are low speed velocity streaks and quasi-streamwise vortices. Both of these features are considered important to the self sustaining mechanism of wall turbulence [15]. Hence, it is expected that these will be affected by the drag reducing effect of polymers. To quantify these effects, detailed spatial measurements of the near wall turbulence are required. From these spatial measurements, quantities such as two point velocity correlations, wall normal vorticity, identification of near wall vortical structures and two dimensional scatter plots of velocity fluctuations are obtained.

A two point correlation of steamwise velocity in the spanwise direction is used to obtain an estimate of the streak spacing. The correlation function C(r), defined as

$$C(r) = \frac{\langle (u(z)u(z+\Delta z))^2 \rangle}{\langle u(z)^2 \rangle}$$

has a minimum at one half the streak spacing. Figure 8(a) shows C(r) as measured for water and drag reductions of 33% and 67% at $y^+ \approx 15$. The spanwise streak spacing normalized by the streak spacing measured in water at the same y^+ is plotted in figure 8(b). The data is in good agreement with the correlation obtained by Oldaker and Tiederman [2] as a best fit to data obtained from flow visualization studies in polymer drag reduced flow. The coarsening of the low speed streaks with increasing drag reduction is apparent in figure 5.

Turbulent structures are identified in the PIV vector plots using techniques suggested by Adrian et al. [12]. Figures 5(a) and 5(b) show the low pass filtered fluctuating velocity fields with enstrophy (vorticity squared) plotted as the contoured background. Regions of high enstrophy are correlated with the wall normal vortical structures, identified as regions of swirling motion in the vector fields. The plots show a drastic reduction in the numbers and strength of these near wall vortical structures with increasing drag reduction. These wall normal structures with a wall normal component of vorticity are likely a slice through the quasi-streamwise vortices which are slightly inclined to the wall and numerous in near wall turbulence. Further evidence of this weakening of near wall structure is obtained from the scatter plots of u'^+ and w'^+ shown in figure 9. Figure 9(a) corresponds to the scatter plot of the velocity fluctuations in water and figure 9(b) in polymer drag reduced flow near MDR (67% drag reduction). In water, large spanwise fluctuations are correlated with positive fluctuations of the streamwise velocity, giving rise to an asymmetric shape of the plot. At 67% drag reduction, the scatter plot is much more symmetric. Differencing the scatter plots as shown in figure 9(c) shows that the action of the polymer is to mitigate the large spanwise fluctuations that are correlated with large streamwise fluctuations. This further indicates that the quasi streamwise vortices, primarily responsible for this correlation, are weakened due to the action of the polymer.

Simultaneous PIV and PLIF in the x-y plane

Simultaneous PIV and PLIF measurements are made in the x-y plane to study the distribution of the injected polymer solution. The dye mixed with the polymer solution is assumed to faithfully follow the polymer solution and any differences between the dye

and polymer are assumed to be insignificant. Figure 10(a) shows a sample snapshot of a PLIF image obtained for flow with drag reduction of 65% (near MDR). At this downstream location, (2m from injection), most of the polymer stays localized very close to the wall. Figure 10(b) shows PIV data obtained at the same time as the PLIF image was taken plotted on top of the PLIF image. Apparent is a direct correlation between regions of high polymer concentration and velocity field. This implies that polymer is still effective i.e. high drag reductions occur even at low homogenous concentration. A measure of the concentration at every pixel in the image was obtained by comparing the intensity at that point with the calibration. Analysis of 100 such images provides a measure of the mean and root mean square concentrations as shown in figure 11. Three important attributes are apparent from this graph: (i) The mean concentration of the polymer in the near the wall is low – 25ppmw. (ii) Most of the polymer resides in less than 25% of the thickness of the boundary layer. (iii) The polymer concentration fluctuations across the interrogation region are large. Overall, these results imply poor mixing of the polymer which happens to be advantageous for drag reduction.

Figure 12 shows, in physical coordinates, a comparison of the mean velocity profile for water and near MDR drag reduced flow obtained from PIV measurements in the x-y plane. Also plotted in the figure is the expected velocity field at MDR, as measured in channel flow at homogenous concentration [11]. From the figure, it is seen that the velocity profile is significantly modified near the wall and closely follows the profile observed in drag reduced homogeneous flow. Away from the wall it reverts back to the profile closely matching that of water, implying that the effect of the polymer on the turbulence very close to the wall is enough to achieve large drag reductions. Figure 13 shows the Reynolds stress profiles for 0%, 33% and 65% drag reductions plotted in physical units. The Reynolds stress close to the wall drops by a large amount (~ 8 x) as drag reduction increases. The large reduction in the Reynolds stress near the wall has been noted in past studies [11]. Again, the present experiments differ from the experiments in homogeneous channel flow, using an ocean of polymer, in the behavior of the Reynolds stress profile away from the wall. Experiments in homogeneous channel flows have measured Reynolds stress to be almost zero across the entire channel at near MDR condition. In the present experiment, away from the wall, the drop in the magnitude of Reynolds stress is marginal. Figure 14 shows a plot of the turbulent energy production across the boundary layer as measured for water, 33% and 65% drag reduction. The action of the polymer close to the wall is to drastically curtail the production of turbulent energy. This effect increases with increasing drag reduction. Near MDR conditions there is almost no production of turbulent energy close to the wall. Away from the wall, there is no change in the trend of turbulent kinetic energy production. The difference observed between boundary layers with slot injection and channel flow with homogeneous concentrations leads one to believe that the polymer-turbulence interactions away from the wall do modify the turbulence there, but this modification has little effect on the wall shear stress – in this sense, the achievement of MDR in flows with polymer addition is not unique.

Discussion

The turbulence data obtained from PIV in the x-z plane indicates that the action of the polymer is to significantly modify the near wall turbulence structure which is

manifested as reduced drag. The structure of the near wall turbulence is modified by presence of the polymer in the flow with the extent of the modification increasing with drag reduction. Low speed streak splitting and merging is inhibited and the spanwise oscillations of the streaks in the boundary layers are dampened due to the polymer-turbulence interaction. Spanwise oscillations of these streaks are damped and streak thickening is also observed. Further, the near wall vortices are also significantly reduced by the presence of polymer. The scatter plots of streamwise and spanwise velocity fluctuations, along with plots of enstrophy, show that the large spanwise fluctuations which are correlated with large streamwise fluctuations are dampened by the presence of the polymers. Simultaneous PLIF and PIV in the x-y plane show that there is a close correlation between the presence of polymer and structure in the near wall boundary layer.

The turbulence statistics obtained from the PIV in both the x-z and the x-y planes indicate that the turbulence statistics in injected boundary layers are quite different from those observed in homogeneous channel flow in spite of the fact that similar drag reductions can be achieved in both cases. This is further proven by the PLIF images which show that it is sufficient to affect only a small part of the near wall boundary layer for attaining high drag reduction. These important differences have also been measured by Petrie and Fontaine [13]. The effect of the polymer on the Reynolds stress and turbulent kinetic energy in the near wall regions of the boundary layers is quite severe. The decrease in the turbulent kinetic energy production near the wall has a direct consequence in the reduction of the number and strength of the near wall vortices and hence results in reduced shear stress on the wall.

Important Finds and Conclusion

These present measurements were able to provide quantitative measures of the flow changes with polymer addition and have shown several results which are particularly important to the understanding of the drag reduction phenomenon. These are listed here:

(i)   We have demonstrated that PIV can be successfully used in a turbulent boundary layer and reproduces all the classical measurements obtained previously by Laser Doppler Velocimetry (LDV) measurements.

(ii)   Results show that sub-layers streaks are coarsened and wall-normal enstrophy is reduced with polymer injection, while Reynolds stress is decreased.

(iii)   Polymers injected into a turbulent boundary layer remain close to the wall for long distances downstream on the injection location, unlike dye injected into a boundary layer.

(iv)   High drag reductions - close to values near the Maximum Drag Reduction Asymptote - are attainable with polymer only close to the wall so that "oceans" of polymer are not necessary for the attainment of high drag reductions. This result is important to boundary layer injection experiments in practical external flow situations.

(v)   MDR appears to not be a unique state, namely it can be achieved via an "ocean" of polymer which is homogeneously distributed as well as via wall injection where the polymer is inhomogeneously distributed.

These results argue for a detailed set of measurements from the injection station to the entire length of the flat plate to include the development length, steady state region and depletion region. Such results will be important for the future development of predictive models.

Significant Hardware Development

The present work required the development of PIV and PLIF for application close to a wall. In addition, during the course of this work the water tunnel had to be moved from one location to another due to the shutting down of the original laboratory for earthquake repairs. This necessitated a full dismantling and reassembly of the water tunnel facility used for the work.

Special Conditions for Further Research

The results presented here were all obtained at a single measurement station 2 m downstream of the injection slot. This was chosen since the boundary layer thickness was a maximum at that station. In the future measurements will be needed along the length of the boundary layer, implying a need for improved resolution. An additional need is for improved velocity statistics. In the present work, data is acquired into computer memory and then transferred to disc while the polymer injection continues – during this time, no further data is acquired. The use of direct data writing to hard disc will alleviate this problem and allow much greater fidelity in the measured statistics. The dataset possible with such improvements will be the first of its kind to allow comparison with numerical simulations.

Bibliography

[1] Virk, P.S., 1975, "Drag Reduction Fundamentals", *AICHE J.*, **21**, pp 625-656

[2] Oldaker, D.K., Tiederman, W.G., 1977, "Structure of the turbulent boundary layer in drag reducing pipe flow", *Phys. Fluids*, **20**, pp S133-S144.

[3] Fontaine, A.A., Petrie, H.L., and Brungart, T.A., 1992, "Velocity Profile Statistics in a Turbulent Boundary Layer with slot injected Polymer," *J. Flu. Mech*, **238**, pp 435-466.

[4] Warholic, M.D., Heist, D.K., Katcher, M., Hanratty, T.J., 2001, "A Study with Particle Image Velocimetry of the Influence of Drag Reducing Polymers on the Structure of Turbulence", *Exp. Fluids*, **31**, pp 474-483.

[5] Henck, R.W., 1990, "An Experimental Investigation of the Fluid Mechanics of an Unsteady, Three Dimensional Seperation", *PhD Thesis*, Stanford University.

[6] Naqwi, A.A., Reynolds, W.C., 1991, "Measurements of Turbulent wall Velocity gradients using cylindrical waves of laser light", *Exp. Fluids*, **10(5)**, pp 257-266.

[7] Keane, R.D., Adrian, R.J., Zhang, Y., 1995, "Super-resolution particle Imaging velocimetry", *Meas. Sci. Tech.*, **6**, pp 754-768.

[8] Hart, D.P., 2000, "PIV error correction", *Exp. Fluids*, **29**, pp 13-22.

[9] Virk, P.S., Merril, E.W., Mickley, H.S., Smith, K.A., Mollo-Christensen, E.L., 1967, "The Toms Phenomenon – turbulent pipe flow of dilute polymer solutions", *J. Flu. Mech*, **30**, pp 305-328.

[10] Spalart, P.R., 1988, "Direct Simulation of a Turbulent boundary layer upto R_θ = 1410", *J. Flu. Mech*, **187**, pp 61-98.

[11] Warholic, M.D., Massah, H., Hanratty, T.J., 1999, "Influence of drag reducing polymers on turbulence, effects of Reynolds number, concentration and mixing", *Exp. Fluids*, **27**, pp 461-472.

[12] Adrian, R.J., Christensen, K.T., Liu, Z.C., 2000, "Analysis and interpretation of instantaneous turbulent velocity fields", *Exp. Fluids*, **29**, pp 275-290.

[13] Petrie, H.L., Fontaine, A.A., 1996, "Comparison of turbulent boundary layer modification with slot injected and homogeneous drag reducing polymer solutions", *ASME Fluids Engg. Div. Conference*, **237**, pp 205-210.

[14] Westerweel, J., 1994, "Efficient detection of spurious vectors in particle image velocimetry data sets." *Exp. Fluids*, **16**, pp 236-247.

[15] Kline, S.J., Reynolds, W.C., Schraub, F.A., Runstadler, P.W., 1967, "The Structure of Turbulent Boundary Layers", *J. Flu. Mech*, **30**, pp 741-773.

Re_θ	U_∞ [m/s]	θ	u^* [m/s]	C_i [ppmw]	C_h [ppmw]	%DR
1330	0.460	2.95	0.0201	100	0.15	33
1330	0.460	2.95	0.0201	100	0.50	45
1371	0.485	2.97	0.0211	500	0.70	50
1414	0.495	3.01	0.0219	500	1.40	67

Table 1: Boundary layer and polymer parameters

Figure 3: Schematic of the x-y plane PIV and PLIF measurement station
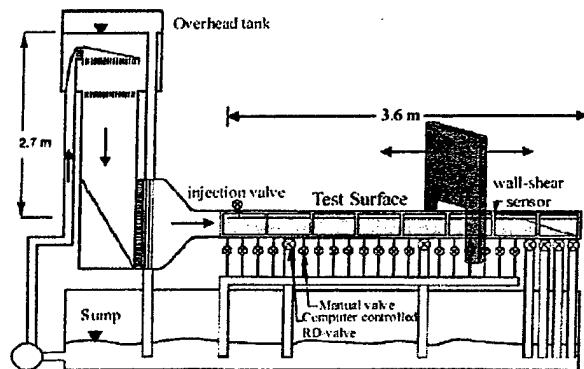
Figure 1: Schematic of the experimental facility
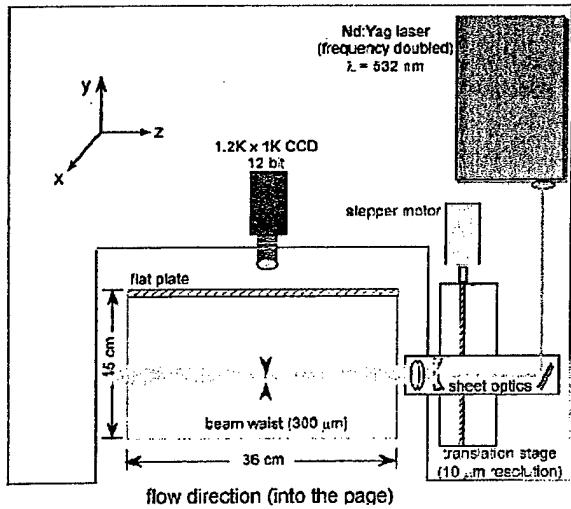
Figure 2: Schematic of the x-z plane PIV measurement station
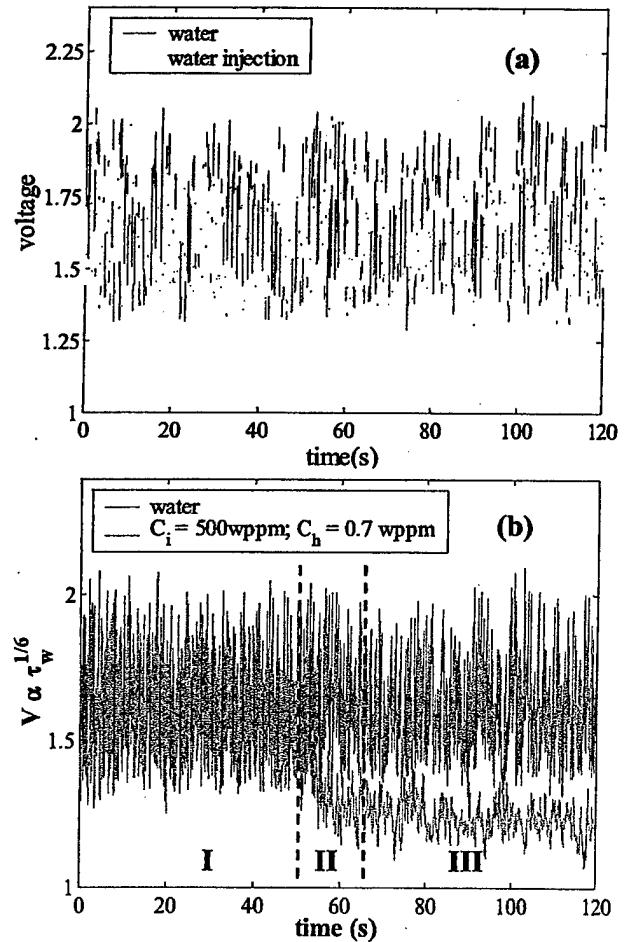
Figure 4: Voltage trace from thermal shear stress sensor

11

(a)

(b)
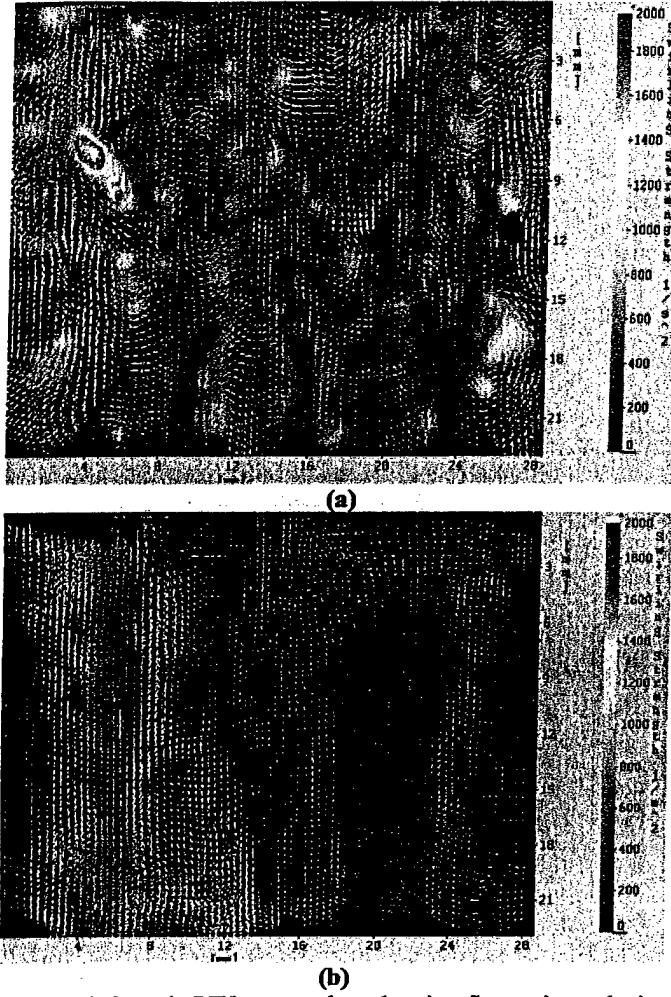
Figure 5: Sample PIV vector plots showing fluctuating velocity and enstrophy in (a) water, 0% drag reduction and (b) with polymer injection, drag reduction of 45%. Flow is from top to bottom.
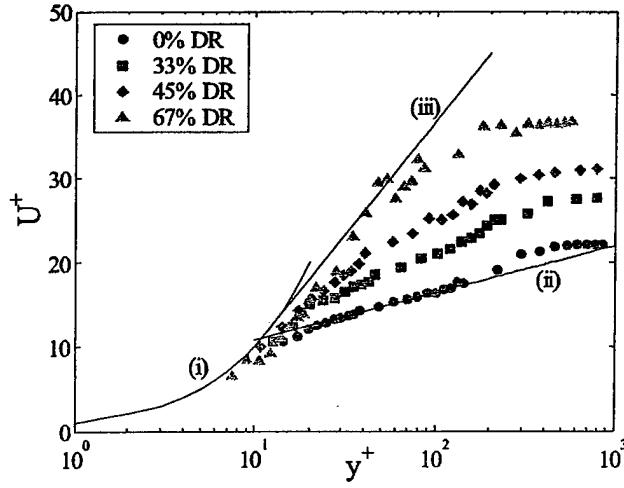
Figure 6: Mean streamwise velocity profile in plus units; (i) U^+ = y^+, (ii) U^+ = 2.44 $\ln(y^+)$ + 5.1, (iii) U^+ = 11.7 $\ln(y^+)$ -17.0 [8]
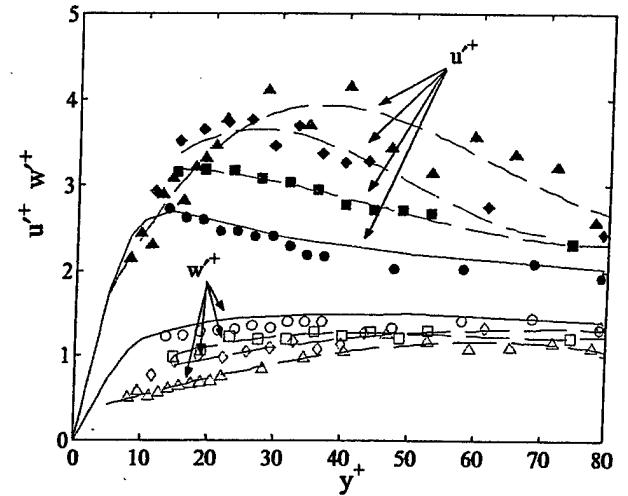

Figure 7: Root mean square velocity profiles plotted in plus units. Closed symbols are for streamwise fluctuations u'^+ and open symbols are for spanwise fluctuations w'^+. The symbols are for the same drag reductions as in figure 6.

(a)

(b)
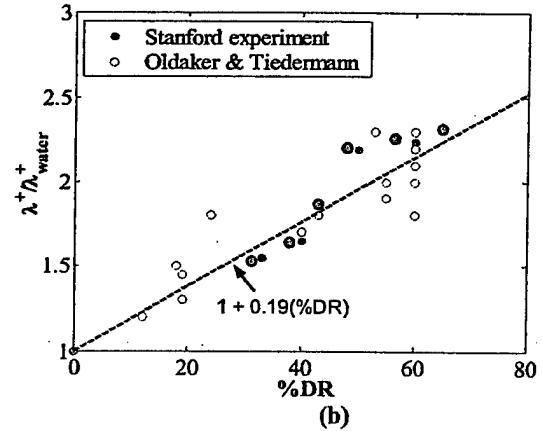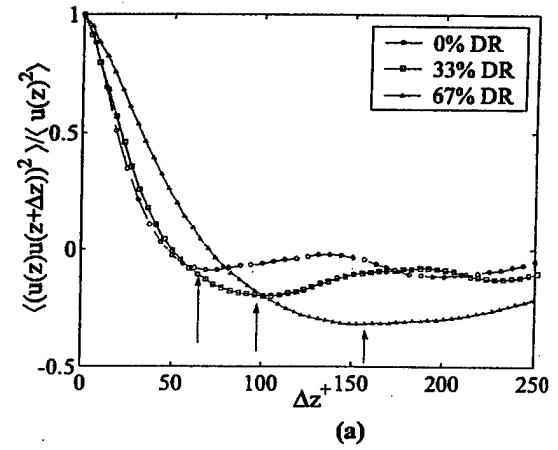
Figure 8: (a) Cross correlation function C(r) measured at y^+ = 15 for various drag reductions. (b)Streak spacing versus drag reduction; dashed line obtained from best fit found by Oldaker and Tiederman [2].

12

(a)

(b)

(c)
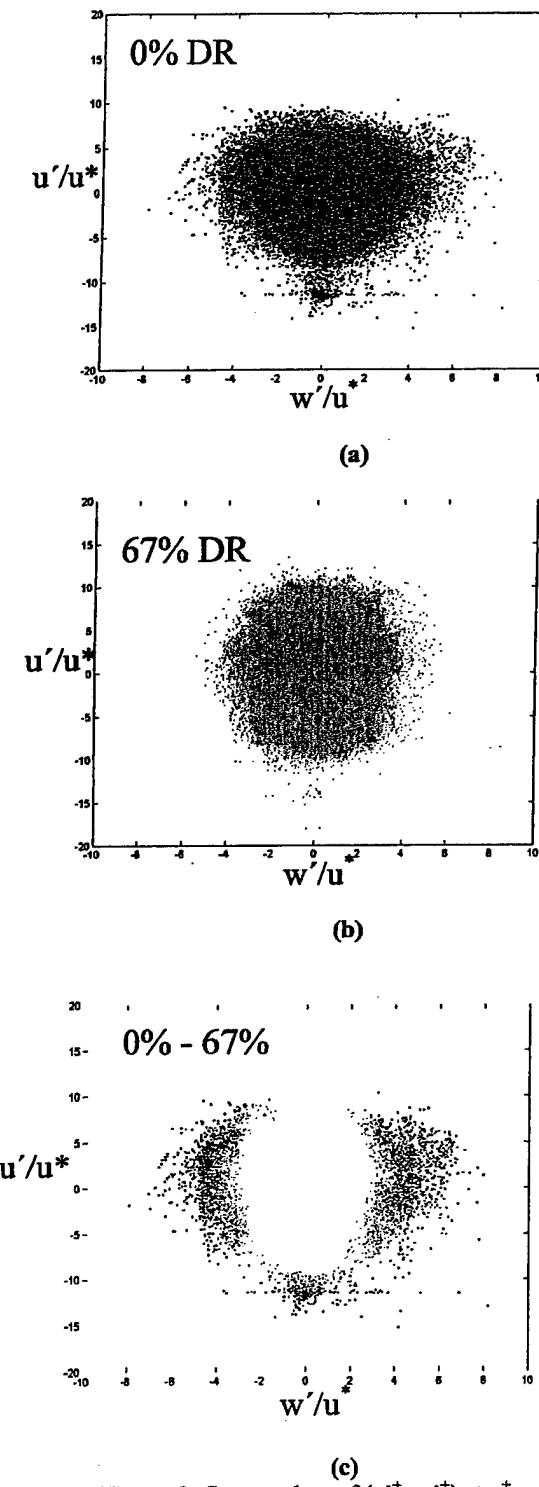
Figure 9: Scatter plots of (u'^+, w'^+) at $y^+ = 15$ in (a) water, (b) 67% drag reduction. (c) is (a) − (b).


(a)

(b)
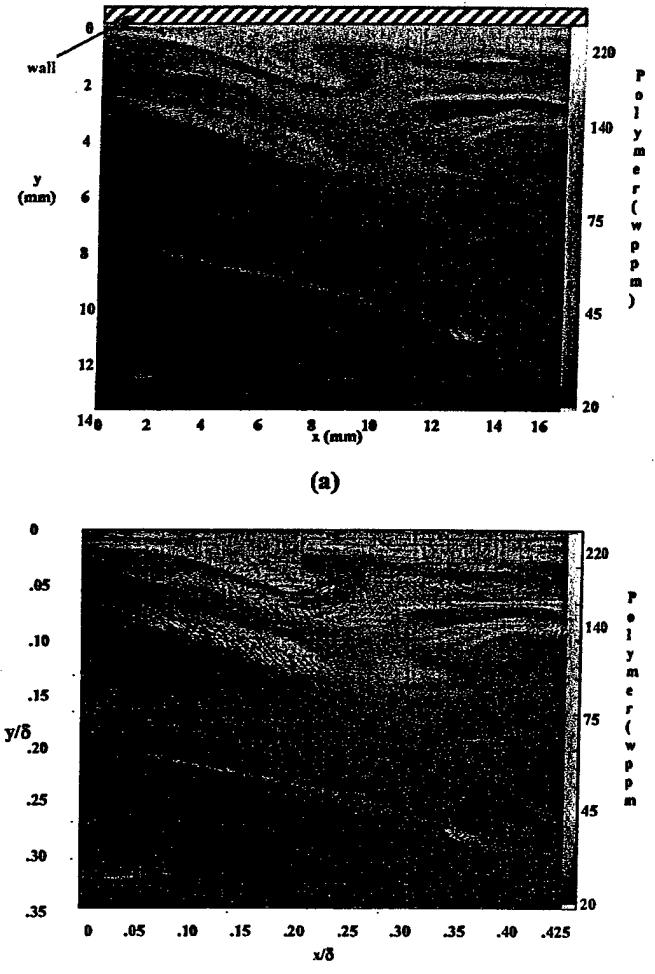
Figure 10: (a) Sample PLIF image of 65% drag reduced flow in the x-y plane. (b) The same image with PIV vector plot overlaid. Flow is from right to left.

13
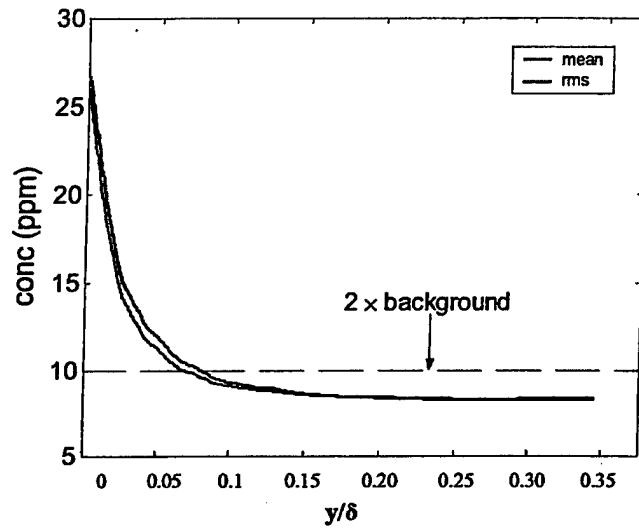
Figure 11: Polymer concentration profile in the x-y plane; ensemble average taken over 100 images.
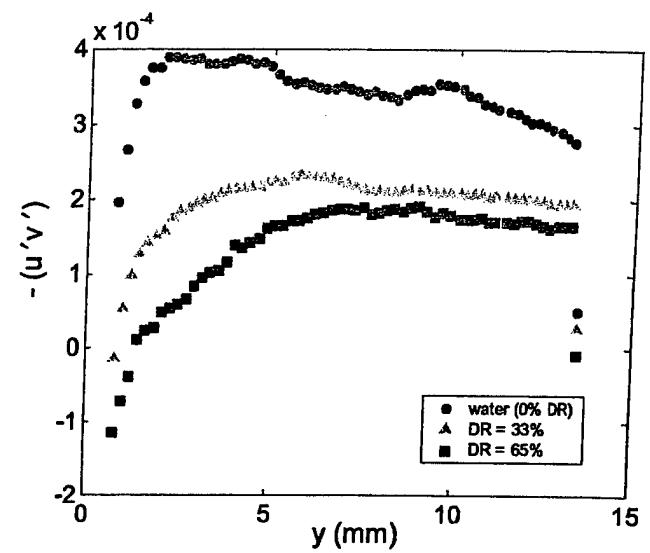

Figure 13: Reynolds stress profiles obtained from PIV in the x-y plane for water, 33% drag reduction and 65% drag reduction
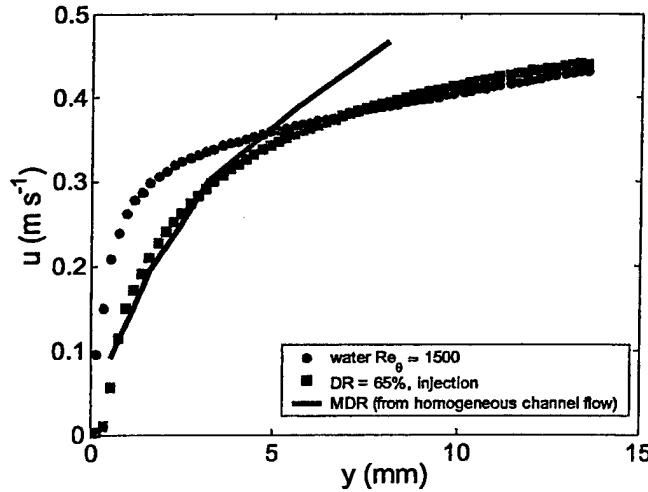

Figure 12: Mean velocity profile obtained from x-y plane data, in physical coordinates, of water, 65% drag reduced flow and inferred MDR profile in homogeneous channel flow.
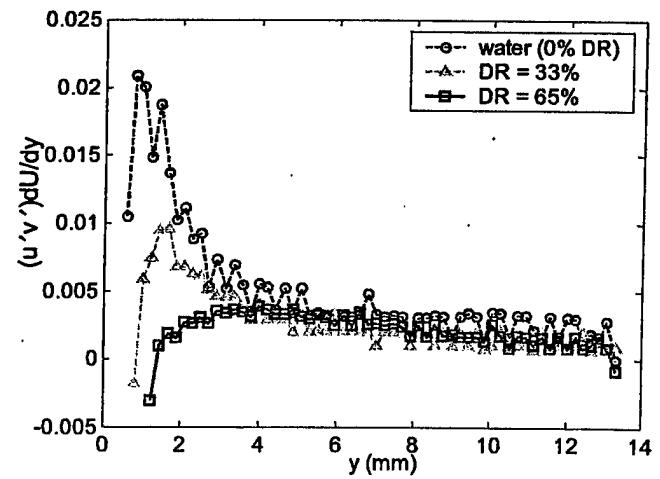

Figure 14: Turbulent kinetic energy profile for water (0% drag reduction), 33% drag reduction and 65% drag reduction

14